

# Electricity Generation based on One-Dimensional Group-III Nitride Nanomaterials

By Xuebin Wang, Jinhui Song, Fan Zhang, Chengyu He, Zheng Hu,\* and Zhonglin Wang\*

In nanoscience and nanotechnology, it is very attractive to develop self-powered nanodevices with the use of nanogenerators replacing batteries. In this way, one could realize independent and continuous operations of implantable biosensors, micro-electromechanical systems, nanorobots and even portable personal electronics.<sup>[1]</sup> Moreover, due to the current energy crisis, it would be even more alluring if the generators can harvest the wasted energy in the environment, such as body-movement, light wind and vibration of acoustic waves.<sup>[2]</sup> By focusing on these applications, great progress has been made in developing piezoelectric nanogenerators using ZnO nanowires,<sup>[3]</sup> CdS nanowires,<sup>[4]</sup> ZnS nanowires,<sup>[5]</sup> PZT nanofibers,<sup>[6]</sup> and GaN nanorods,<sup>[7]</sup> which give great promise for the integration of piezotronics and nanoelectronics.

Group-III nitride semiconductors, highlighted for their tunable, direct band gap and good chemical stability,<sup>[8]</sup> also have a pronounced piezoelectric property owing to their wurtzite crystal structures. In terms of the coupling between their piezoelectric and semiconducting properties, an output power should be generated by scanning an atomic force microscope (AFM) tip in contact mode across 1D group-III nitride nanomaterials. In this study, a family of 1D group-III nitrides, including AlN and AlGaN nanocones, GaN nanorods and InN nanocones, are synthesized through a facile chemical-vapor-deposition (CVD) route based on previous work.<sup>[9]</sup> Increasing electricity generation is demonstrated following the sequence: AlN, AlGaN, GaN and InN, which can be attributed to the increasing piezoelectric potential and carrier density. These results not only extend piezotronics to a new domain of group-III nitrides, but also deepen the understanding of the underlying physics of piezoelectric nanogenerators.

Figure 1 shows scanning electron microscopy (SEM) and transmission electron microscopy (TEM) images of the quasialigned arrays of AlN nanocones, AlGaN nanocones, GaN nanorods and InN nanocones, with diameters at the middle of around 100, 70, 500, and 700 nm, and the lengths of about 2, 1,

3.5, and 4  $\mu\text{m}$ , respectively. The nanostructures preferentially stand perpendicularly on the Si substrates. Due to the relatively large sizes of the GaN nanorods and InN nanocones, their hexagonal intersections are obvious, and are determined by their common family crystal structure.<sup>[10]</sup> The corresponding high-resolution transmission electron microscopy (HRTEM) images and selected-area electron-diffraction (SAED) patterns (insets of Fig. 1b, 1d, 1f, and 1h) indicate that single crystals of the nitrides possess the [001] growth direction. The spacings of 0.266, 0.252, 0.529, and 0.302 nm between the neighboring lattice planes in the HRTEM images are consistent with the  $d_{100}$ ,  $d_{002}$ ,  $d_{001}$ , and  $d_{100}$  spaces of hexagonal AlN, AlGaN,<sup>[11]</sup> GaN, and InN, respectively. X-ray diffraction (XRD) profiles of these samples are shown in Figure 2, and could be indexed to hexagonal wurtzite AlN,  $\text{Al}_{0.33}\text{Ga}_{0.67}\text{N}$  (based on Vegard's law<sup>[12]</sup>), GaN and InN (JCPDS card No 65-0832, 50-0792, 50-1239). The much-stronger intensity of the (002) peak relative to the corresponding standard diffraction pattern indicates preferential growth along the  $c$ -axis,<sup>[9]</sup> in agreement with the SAED patterns.

In the demonstration of piezoelectric responses for the four nitrides samples, the three-dimensional (3D) output-voltage images were recorded when the AFM tip scanned over a  $20\ \mu\text{m} \times 20\ \mu\text{m}$  area of the samples, as shown in Figure 3a, 3c, 3e, and 3g. Sharp voltage pulses were detected for all of the nitride nanostructures, except for AlN. The pulse magnitudes were about 4, 7, and 60 mV for AlGaN, GaN, and InN respectively, much larger than the noise level ( $\sim 0.5$  mV). All of the pulses were negative, if the substrates were grounded as schemed in the insets of Figure 3a. Figure 3b, 3d, 3f, and 3h show a comparison of the line-scan topography profiles (dark curves) and the corresponding output-voltage profiles (blue curves) recorded from one line-scan process. As indicated by the peaks in these profiles, the voltage pulses approximately occurred when the AFM tip scanned across the nanocones/nanorods. This indicates that the discharge took place when the tip contacted with the compressed side of the 1D nanostructures.

Similar to the model of the ZnO-based nanogenerators in the previous study,<sup>[3]</sup> the piezoelectric and semiconducting properties of these nitrides were coupled to produce the piezoelectric output, as schematically illustrated in Figure 4. When a nanorod (or nanocone) is bent by the lateral force, a strain field is created with the left-hand side stretched and the right-hand side compressed (Fig. 4a). A piezoelectric potential is thus created in the nanorod due to the polarization of the ions. The group-III nitride nanostructures synthesized by the CVD route usually grow along the positive  $c$ -axis with a front-terminating layer of metal atoms.<sup>[9,13]</sup> Hence, the piezoelectric potential distribution was

[\*] Prof. Z. Hu, Dr. X. B. Wang, Dr. F. Zhang, Dr. C. Y. He  
Key Laboratory of Mesoscopic Chemistry of MOE and Jiangsu  
Provincial Lab for Nanotechnology, School of Chemistry and  
Chemical Engineering, Nanjing University Nanjing, 210093, China  
E-mail: zhenghu@nju.edu.cn

Prof. Z. L. Wang, Dr. J. H. Song  
School of Materials Science and Engineering, Georgia Institute of  
Technology Atlanta, Georgia 30332, USA  
E-mail: zlwang@gatech.edu

DOI: 10.1002/adma.200903442

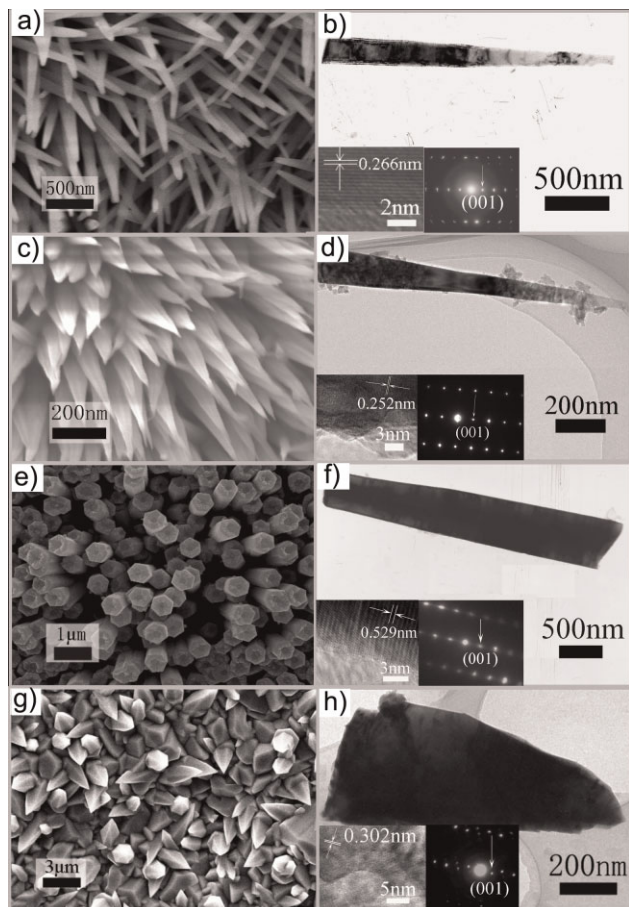


**Figure 1.** Typical SEM images of a) AlN nanocones, c) AlGaIn nanocones, e) GaN nanorods, and g) InN nanocones, and typical TEM images of b) AlN nanocones, d) AlGaIn nanocones, f) GaN nanorods, and h) InN nanocones. The insets show the corresponding HRTEM images and SAED patterns.

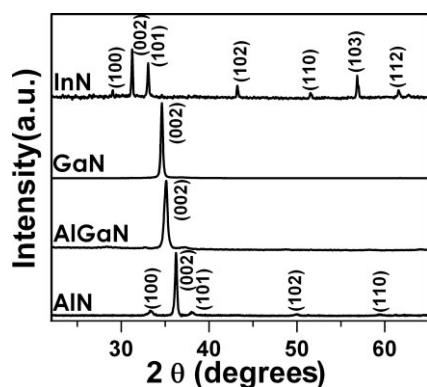


**Figure 2.** The XRD profiles of the synthesized 1D group-III nitride nanostructures on Si substrates.

from zero to a positive maximum along the stretched side, and from zero to a negative maximum along the compressed side of the nanorod. In addition, due to the smaller electron affinity of these n-type nitrides (AlN: zero or even negative;<sup>[9]</sup> GaN: 4.1 eV;<sup>[14]</sup>

InN: 5.8 eV<sup>[15]</sup>) than the work function of Pt (6.1 eV), a Schottky barrier exists between the Pt-coated tip and the nanorod, as represented by the rectifying character of the Pt-GaN junction shown in Figure 4b. Consequently, as the tip touches and bends the nanorods (Fig. 4c and 4e), the Schottky barrier is reverse-biased and no current flows across the interface. On the contrary, as the tip scans over the top of the nanorod and touches the compressed side (Fig. 4d and 4f), the built-up negative potential forwardly biases the Schottky barrier, which causes the free electrons outside the nanorod to flow in and neutralize the polarized charges. Then, a voltage drop is detected on the load, which is the process of power generation. In a word, the piezoelectric effect creates positive and negative potential regions in the nanorod, and the Schottky barrier serves as a gate in the nanogenerator to accumulate and release the charges. If there were no Schottky barrier, the slowly leaked current would be in the noise level and would not be detected beyond the background.

For an ideal static model without considering its conductivity, the potential distribution along the piezoelectric semiconductor induced by the piezoelectric effect depends on the length ( $L$ ) and diameter at the middle ( $a$ ) of the nanostructure, the maximum deflection ( $\gamma_m$ ), the piezoelectric constant ( $e_{33}$ ) and the relative dielectric constant ( $k_{r,\perp}$ ), with the relationship given in Equation (1) as an estimation ( $k_0$  is the permittivity of vacuum):<sup>[3,16]</sup>

$$V_S^\pm \approx \frac{3e_{33}}{4k_0k_{r,\perp}} \cdot \left(\frac{a}{L}\right)^3 \cdot \gamma_m \quad (1)$$

To calculate the magnitudes of the electric pulses, we have  $\gamma_m = 1.1, 0.55, 1.1,$  and  $1.3 \mu\text{m}$  (see Supporting Information, SI 1),  $e_{33} = 1.46, 0.97, 0.73,$  and  $0.97 \text{ C m}^{-2}$ <sup>[17,18]</sup> and  $k_{r,\perp} = 9.14, 9.98, 10.4,$  and  $9.3$ ,<sup>[18,19]</sup> for AlN, AlGaIn, GaN and InN respectively. Then, the maximum potentials at the surface are 2, 2, 20, and 60 V for the corresponding nitrides. These potentials are large enough to drive the Pt-nitride Schottky barrier and the output signals observed are the difference in the Fermi levels between the two electrodes connected to the Pt tip and the nitride nanorods/nanocones. The calculated piezoelectric potentials increasing in the sequence AlN, AlGaIn, GaN and InN may produce the increasing output voltage, as observed in the experiments.

It was noticed that the measured voltage signals were always much lower than the calculated ones, which should result from the contact resistance between the Pt and the nitrides, the finite conductivity and the very-small capacitance of the nanocones/nanorods.<sup>[2,20]</sup> Actually, the finite conductivity of the nanocones/nanorods, mainly related to the carrier density for these nitrides, would greatly influence the output voltage. If the free carrier density were too high, the piezoelectric charges would be largely screened and the magnitude of the piezoelectric potential would be reduced, thus decreasing the output voltage. If the carrier density were too low, although the local piezoelectric potential could increase, the output voltage would also decrease due to the much increased inner resistance, and thereafter, the decreased circuit current. Therefore, an optimum conductivity or carrier density is just required to generate a highest output. This picture can be applied to understand the apparent inconsistency of the

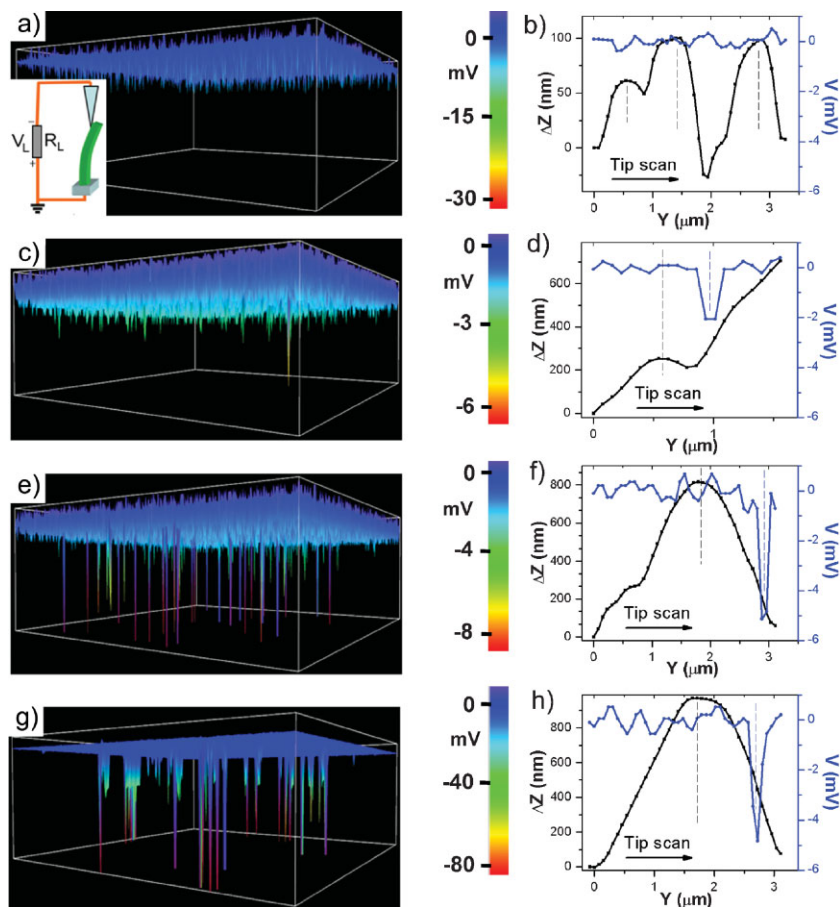


**Figure 3.** 3D electric signal images (left) and corresponding voltage profiles and line-scan topography profiles (right, blue/right, black respectively) of the samples: a,b) AlN; c,d) AlGaN; e,f) GaN; g,h) InN. The inset in Figure 3a shows the measurement scheme of the nanogenerators. The dark dashed lines refer to the times when the AFM tip scans over the top of the nanostructure and the blue ones refer to the time of discharge.

changing electricity generation with conductivity for the ZnO nanogenerators in the previous study<sup>[21]</sup> and the nitride nanogenerators in this study.

For the nanogenerators of ZnO nanowires, a decreasing output was observed with increasing carrier density,<sup>[21]</sup> which can be ascribed to the high carrier densities of the ZnO nanowires over the optimum one. To the contrary, the nanogenerators of the family of nitrides here demonstrate an increasing output with increasing carrier density, in the sequence of AlN, AlGaN, GaN, and InN ( $\sim 10^{-11}$ – $10^{-13}$ ,  $\sim 0.5$ ,  $\sim 6$ – $12$  and  $\sim 200$ – $300 \text{ } \Omega^{-1} \text{ cm}^{-1}$  for the undoped AlN,  $\text{Al}_{0.35}\text{Ga}_{0.65}\text{N}$ , GaN, and InN) respectively,<sup>[19,22]</sup> as shown in Fig. 3. This new phenomenon should be attributed to their low carrier densities, below the optimum. Specifically, AlN nanogenerators produce no output due to their extremely poor conductivity preventing the flow of current. On increasing the conductivity for this series, the inner resistance of the used nanomaterial decreases accordingly. As a result, the voltage consumed by the inner resistance becomes less and less, and the voltage output increases gradually (Fig. 3). Hence, InN, with the highest carrier density, generated the largest output of 60 mV in this series of nitride nanogenerators. According to the

preceding analysis and discussion, it is expected that an integration of the high piezoelectric effect with an optimum conductance would be the next step in enhancing the output of nanogenerators. Actually, from Equation (1), it could be inferred that preparing perpendicularly aligned nanostructures with a large  $a/L$  ratio by using a piezoelectric material with a small Young's modulus ( $Y$ ) is beneficial for achieving a high piezoelectric potential ( $SI$  2). For group-III nitrides, InN has the smallest  $Y$ , and, meanwhile, a suitable conductivity for a voltage output, as aforementioned. Hence, it is suggested that more effort should be devoted to the highly oriented InN arrays with the large  $a/L$  for further optimizing of the performance of nanogenerators.

In summary, a family of 1D group-III nitrides, including AlN, AlGaN, GaN, and InN, have been synthesized through a facile CVD route. With these nanomaterials, piezoelectric generation has been extended to a new domain of group-III nitrides by systematic examination of their nanogenerators. The increasing output is demonstrated following the sequence: AlN, AlGaN, GaN, and InN, which can be attributed to the increasing carrier density and piezoelectric potential. The output change with carrier density for these nitride nanogenerators is opposite to the case for the previously investigated ZnO nanogenerators. This new phenomenon indicates that, for a nanomaterial whose conductivity is below an optimum value, the output of its piezoelectric nanogenerator is dominated by the consumed voltage at the nanomaterial, which deepens the understand-

ing of the underlying physics of piezoelectric nanogenerators. The results suggest that an integration of high piezoelectric effect with an optimum conductance should be a promising strategy to enhance the output of nanogenerators.

## Experimental

The 1D group-III nitride nanostructures were synthesized in a horizontal tubular furnace with two temperature zones. Typically, an anhydrous group-III chloride was placed at the low-temperature (low- $T$ ) zone, and a Ni-coated Si (111) substrate was placed at the center of the high-temperature (high- $T$ ) zone for deposition. In Ar, the chloride was vaporized in the low- $T$  zone at the designed temperature ( $\text{AlCl}_3$ : 135 °C;  $\text{GaCl}_3$ : 110 °C;  $\text{InCl}_3$ : 470 °C) and the material was subsequently transported to the high- $T$  zone to react with  $\text{NH}_3$  ( $200 \text{ cm}^3 \text{ min}^{-1}$ ) for 4 h at the designed temperature (800, 700, 850, and 550 °C for the synthesis of AlN, AlGaN, GaN, and InN, respectively). The group-III nitride nanostructures were then obtained on the substrates. These samples were characterized by XRD (Philips X' Pert Pro), SEM (Hitachi FE-SEM 4800), TEM (JEOL-JEM 1010) and HRTEM (JEOL-JEM 2100) with SAED.

The piezoelectric response was examined using AFM (model MFP-3D from Asylum Research) in contact mode [3]. The nitride samples were fixed

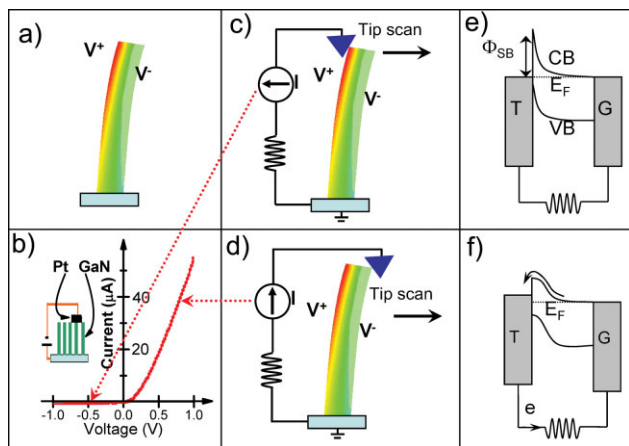


**Figure 4.** Scheme for electricity generation using 1D group-III nitride nanostructures. a) Potential distribution along the nanorod after being deflected. b) The rectifying character of the Pt-GaN Schottky junction. The inset to Figure 4b shows the corresponding measurement scheme. c) Contact mode between the AFM tip and the nanorod corresponding to the reverse-biased Schottky junction. The process separates and maintains the charges, as well as builds up the potential. d) Contact mode corresponding to the forward-biased Schottky junction. This process discharges and generates the electric current. e) and f) Energy diagrams of a nanorod with one end grounded (G) and the other end scanned by a conductive AFM tip (T), corresponding to the cases described in Figure 4c and Figure 4d.  $\Phi_{SB}$  denotes the height of the Schottky barrier.

on a piece of metal plate with silver paste, with the thin nitride film formed at the bottom as a common grounded electrode. The free ends of the nitride nanostructures were deflected consecutively using a Pt-coated silicon tip (14  $\mu\text{m}$  in height with an apex angle of  $70^\circ$ , from Olympus) with a scanning speed of  $12 \mu\text{m s}^{-1}$  at a constant normal force of 5 nN. The output-voltage signal was measured on a  $5 \times 10^8 \Omega$  resistor connected in the closed circuit.

The transport measurements of the samples mimicked those of the piezoelectric measurements. One end of the 1D nanostructure was fixed with silver paste, while the other was contacted with the Pt-coated silicon tip. The current-voltage ( $I$ - $V$ ) characterization was performed with an applied voltage of  $-1$  to  $+1$  V.

## Acknowledgements

This work was financially supported by NSFC (20525312, 20833002), the "973" program (2007CB936300), DARPA (Army/AMCOM/REDSTONE AR, W31P4Q-08-1-0009), BES DOE(DE-FG02-07ER46394), the Air Force

Office (FA9550-08-1-0446), and Emory-Georgia Tech CCNE from NIH, NSF (DMS0706436, CMMI 0403671). X.B.W., J.H.S. and F.Z. contributed equally to this work. Supporting Information is available online from Wiley InterScience or from the author.

Received: October 7, 2009  
Revised: November 22, 2009  
Published online: March 5, 2010

- [1] Z. L. Wang, *Mater. Sci. Eng. R* **2009**, *64*, 33.
- [2] Z. L. Wang, *Adv. Funct. Mater.* **2008**, *18*, 1.
- [3] Z. L. Wang, J. H. Song, *Science* **2006**, *312*, 242.
- [4] Y. F. Lin, J. H. Song, Y. Ding, S. Y. Liu, Z. L. Wang, *Appl. Phys. Lett.* **2008**, *92*, 022105.
- [5] M. Y. Lu, J. H. Song, M. P. Lu, C. Y. Lee, L. J. Chen, Z. L. Wang, *ACS Nano* **2009**, *3*, 357.
- [6] S. Y. Xu, Y. Shi, *Mater. Res. Soc. Symp. Proc.* **2007**, *1034*, 1034-K11-06.
- [7] W. S. Su, Y. F. Chen, C. L. Hsiao, L. W. Tu, *Appl. Phys. Lett.* **2007**, *90*, 063110.
- [8] V. Dmitriev, A. Usikov, in: *III-Nitride Semiconductor Materials*, (Ed: Z. C. Feng), Imperial College Press, London, UK **2006**, Ch. 1, pp. 6-7.
- [9] C. Liu, Z. Hu, Q. Wu, X. Z. Wang, Y. Chen, H. Sang, J. M. Zhu, S. Z. Deng, N. S. Xu, *J. Am. Chem. Soc.* **2005**, *127*, 1318.
- [10] a) Q. Wu, Z. Hu, X. Z. Wang, Y. N. Lu, X. Chen, H. Xu, Y. Chen, *J. Am. Chem. Soc.* **2003**, *125*, 10176; b) X. Chen, J. Ma, Z. Hu, Q. Wu, Y. Chen, *J. Am. Chem. Soc.* **2005**, *127*, 7982.
- [11] Assuming the crystal lattice of  $\text{Al}_x\text{Ga}_{1-x}\text{N}$  varies linearly with the content of Al, then  $x = 0.39$  here.
- [12] L. Vegard, *Z. Phys.* **1921**, *5*, 17.
- [13] a) H. Morkoc, *Mater. Sci. Eng. R* **2001**, *33*, 135; b) J. Komiyama, K. Eriguchi, Y. Abe, S. Suzuki, H. Nakanishi, T. Yamane, H. Murakami, A. Koukitu, *J. Cryst. Growth* **2008**, *310*, 96.
- [14] S. Arulkumaran, T. Egawa, H. Ishikawa, T. Jimbo, M. Umeno, *Appl. Phys. Lett.* **1998**, *73*, 809.
- [15] W. Walukiewicz, K. M. Yu, S. X. Li, R. E. Jones, J. W. Ager, E. E. Haller, H. Lu, W. J. Schaff, in *Proc. E-MRS Fall Meeting*, Pielaszek Research Warsaw **2005**.
- [16] Y. F. Gao, Z. L. Wang, *Nano Lett.* **2007**, *7*, 2499.
- [17] F. Bernardini, V. Fiorentini, D. Vanderbilt, *Phys. Rev. B: Condens. Matter* **1997**, *56*, R10024.
- [18] The  $\epsilon_{33}$  and  $k_{r\perp}$  values of  $\text{Al}_{0.33}\text{Ga}_{0.67}\text{N}$  are estimated by the linear interpolation with the corresponding data of AlN and GaN.
- [19] O. Madelung, *Semiconductors: Data Handbook*, Springer Press, Berlin, Germany **2004**, pp. 204-568.
- [20] a) Z. L. Wang, *Adv. Mater.* **2009**, *21*, 1311; b) Y. F. Gao, Z. L. Wang, *Nano Lett.* **2009**, *9*, 1103.
- [21] J. Liu, P. Fei, J. H. Song, X. D. Wang, C. S. Lao, R. Tummala, Z. L. Wang, *Nano Lett.* **2008**, *8*, 328.
- [22] J. Li, K. B. Nam, J. Y. Lin, H. X. Jiang, *Appl. Phys. Lett.* **2001**, *79*, 3245.